Orientational Order in Dense Colloidal Liquids and Glasses

Yiming Xia,[1,2,*] Xiunan Yang,[1,2,*] Junchao Huang,[3] Rui Liu,[1,2] Ning Xu,[3] Mingcheng Yang,[1,2,4] and Ke Chen[1,2,4,†]
[1]*Beijing National Laboratory for Condensed Matter Physics and Key Laboratory of Soft Matter Physics, Institute of Physics, Chinese Academy of Sciences, Beijing 100190, People's Republic of China*
[2]*University of Chinese Academy of Science, Beijing 100049, People's Republic of China*
[3]*Hefei National Research Center for Physical Sciences at the Microscale, CAS Key Laboratory of Microscale Magnetic Resonance and Department of Physics, University of Science and Technology of China, Hefei 230026, People's Republic of China*
[4]*Songshan Lake Materials Laboratory, Dongguan, Guangdong 523808, People's Republic of China*

(Received 21 November 2022; revised 7 June 2023; accepted 30 August 2023; published 20 September 2023)

We construct structural order parameters based on local angular and radial distribution functions in dense colloidal suspensions. All the order parameters show significant correlations to local dynamics in the supercooled and glass regime. In particular, the correlations between the orientational order and dynamical heterogeneity are consistently higher than those between the conventional two-body structural entropy and local dynamics. The structure-dynamics correlations can be explained by a excitation model with the energy barrier depending on local structural order. Our results suggest that in dense disordered packings, local orientational order is higher than translational order, and plays a more important role in determining the dynamics in glassy systems.

DOI: 10.1103/PhysRevLett.131.128201

Glassy systems such as supercooled liquids and amorphous solids are often referred to as "disordered" matters, due to the lack of apparent long-range order in their structures. From the ensemble averaged radial distribution functions (RDFs), the structures of flowing liquids and solid glasses are essentially identical, despite qualitative changes in the thermodynamical properties and orders of magnitudes differences in relaxation dynamics [1,2]. This absence of clear structure-property connections in amorphous materials challenges the long-standing paradigm in condensed matter physics. To re-establish this connection, it has been proposed that certain nonperiodic structural order, or amorphous order exists in glasses and supercooled liquids. The development of amorphously ordered structures during glass transitions can qualitatively explain some of the fundamental phenomena in glass physics, including the rapid slowing down of dynamics and dynamical heterogeneity [3–13]. However, the details of the amorphous structural order remain unclear. As they are spatially nonperiodic, they are hard to detect by most scattering-based experimental techniques. Even when the atomic positions can be readily extracted using transmission electron microscope or atomic electron tomography [14,15], no libraries of structures are available to distinguish ordered structures from disordered background.

Many proposals have been put forward to identify amorphously ordered structures in glassy systems, and to establish credible links to dynamics or mechanical properties of glasses [16]. Symmetry-based models [17–21] determine the local structural order by comparing configurations to high-symmetry templates including crystalline structures. Point-to-set [22–26] analyses are employed to detect the length scale of ordered structures without knowing the details of atomic arrangements in the ordered domains. Recently, machine-learnt softness [27–31] and local structural entropy S_2 [17,32–34] show strong predicting power for local deformations in binary liquids or glasses. Both the softness and S_2 rely heavily on the local RDFs [27,32] that are averaged over all directions under the assumption of angular isotropy. The actual angular distributions of neighbors around a particle in glasses, however, are rarely uniform, and can vary considerably from one location to another. Such angular anisotropy are particularly significant within the first few neighbor shells where the RDF also exhibits large fluctuations. Tong *et al.* [35–37] discover that an order parameter based on bond angles in the first-neighbor shell, when coarse-grained, can efficiently predict the mobility patterns in glasses over time. Such nonuniformity in angular distributions of neighboring particles contains valuable information regarding the amorphous orders in glasses [38], as structural orders are simply reflections of spatial anisotropies, as in the cases of crystals and the short-range orders in glasses [39].

In this Letter, we extend the conventional two-body structural entropy S_2 to include angular fluctuations, defining a total structural entropy S_a that contains both radial and angular information, and a orientational entropy S_o that depends only on angular fluctuations. All three structural order parameters, S_2, S_a, and S_o, are evaluated locally for each particle in quasi-two-dimensional (quasi-2D) colloidal packings, and are correlated to local dynamics. Of the three order parameters, S_a exhibits the highest

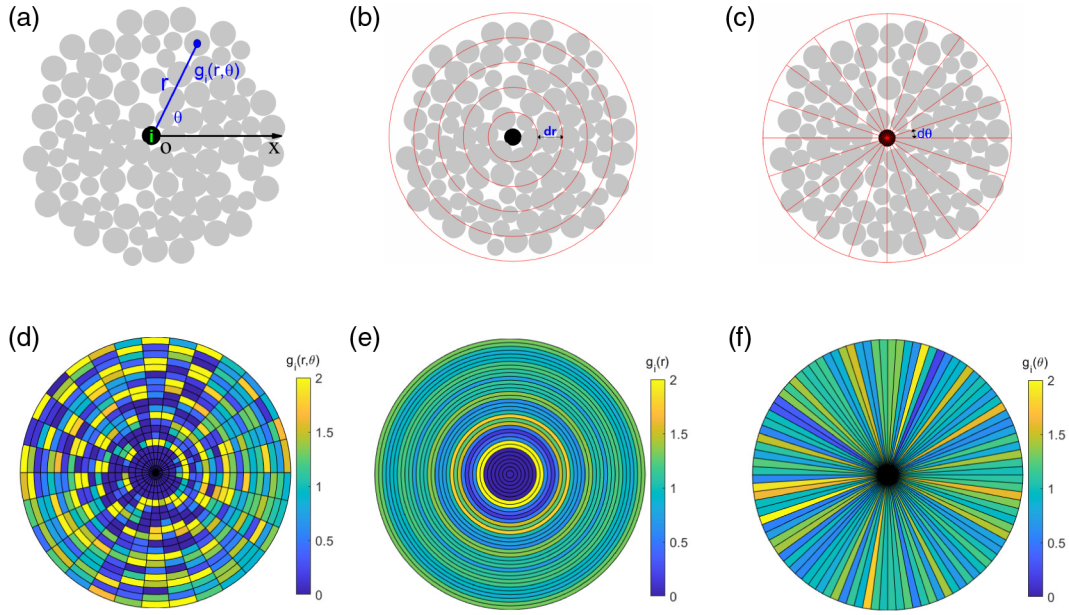

FIG. 1. Local distribution functions in disordered packings. (a) Diagram for the two-parameter local distribution function $g_i(r,\theta)$, with the reference particles i at the center, and the positions of neighboring particles described by polar coordinates (r,θ). (b),(c) Diagrams for radial local distribution functions $g_i(r)$ and $g_i(\theta)$, when the neighboring regions of the reference particles are partitioned into rings or sectors. (d)–(f) Representative distribution functions $g_i(r,\theta)$, $g_i(r)$, and $g_i(\theta)$ for a particle; colors indicate relative probability to the mean.

structure-dynamics correlations, and S_o shows consistently higher correlations to dynamics than S_2 under comparable statistics. All correlation coefficients increase with the packing fraction, which can be understood using a simple excitation model. Our results highlight the important role of the orientational configurations in the structural orders in liquids and glasses, which has been largely overlooked in previous studies.

We perform video-microscopy measurements on colloidal samples. The samples consist of a binary mixture of PNIPAM particles confined between two cover slips, forming a monolayer of quasi-2D colloidal suspensions [40–42]. The diameter ratio of the particles is chosen to be ~1.4 with a number ratio of ~1 to frustrate crystallization at 2D [43–45]. The PNIPAM particles are thermosensitive whose diameters decrease with increasing temperature. During the experiments, the sample packing fraction is tuned *in situ* by an objective heater, from flowing liquids to jammed glasses. The samples are imaged using standard brightfield microscopy at 60 fps. Before data acquisition, the samples are equilibrated on the microscope stage for 3 h. There are ~3500 particles in the field of view, and the particle trajectories are extracted using particle tracking techniques [46]. The vertical fluctuations of the particles are estimated to be 0.15 μm or 12% of the average particle's diameter [41]. Collective drifting of the particles is digitally removed before further analysis.

In the experiments, the position of a neighboring particle relative to a reference particle can be described by the separation r and an orientation angle θ relative to a preset axis (x axis in this Letter), as shown in the diagram in Fig. 1(a). Thus, a two-parameter local distribution function $g_i(r,\theta)$ can be defined as $g_i(r,\theta) = [n(r,\theta)/n_e(r,\theta)]$, where $n(r,\theta)$ is the local number density at (r,θ), and $n_e(r,\theta) = \rho$ is the mean number density of the system. Figure 1(d) plots the local distribution function of a typical particle in the experiment, with different colors corresponding to the values of $g_i(r,\theta)$. It is easy to show that when averaged over θ, one recovers the commonly used radial distribution function $g_i(r) = (1/2\pi)\int_0^{2\pi} g_i(r,\theta)d\theta$. An angular distribution function is defined as the radial average of the local distribution function, with $g_i(\theta) = (2/R^2)\int_0^R g_i(r,\theta)rdr$. In principle, the integral limit R extends to infinity, but in practice the distributions of particles further than 5 diameters are close to the system average. And in our experiments, we limit our analyses to particles more than 5 diameters away from the boundary of the images. Figures 1(b) and 1(c) show the diagram for evaluating $g_i(r)$ and $g_i(\theta)$, respectively. And Figs. 1(e) and 1(f) plot the color-coded $g_i(r)$ and $g_i(\theta)$ with the same total number of bins as $g_i(r,\theta)$ in Fig. 1(d). It is clear that all three local distribution functions are not spatially uniform with considerable fluctuations. In practice, the distribution functions depend on the finite spatial resolution of particle positions and limited statistics in experiments. When the bins are too narrow, the distribution functions suffer from poor statistics, and record largely noises, while too wide bins average out small-scale structural features. We estimate the higher and lower bound of bin numbers based on experimental conditions, and choose a range where the

distribution functions are insensitive to the varying of bin numbers [47].

For each of the three local distribution functions, $g_i(r,\theta)$, $g_i(r)$, and $g_i(\theta)$, a local structural entropy can be defined for each particle i. Specifically, for $g_i(r,\theta)$, we have

$$S_{a,i} = -\frac{k_B}{2}\sum_{u=b,s}\rho_{i,u}\int_0^R\int_0^{2\pi}[g_{i,u}(r,\theta)\ln g_{i,u}(r,\theta) - g_{i,u}(r,\theta)+1]rdrd\theta, \quad (1)$$

where $\rho_{i,u}$ is the number density of big or small particles surrounding particle i, $g_{i,u}(r,\theta)$ is the local distribution function between particle i and particles of type u. Similarly, entropy from the radial distribution is the commonly used two-body structural entropy [54]

$$S_{2,i} = -k_B\pi\sum_{u=b,s}\rho_{i,u}\int_0^R[g_{i,u}(r)\ln g_{i,u}(r) - g_{i,u}(r)+1]rdr \quad (2)$$

and the orientational entropy is defined as

$$S_{o,i} = -\frac{k_B}{4}R^2\sum_{u=b,s}\rho_{i,u}\int_0^{2\pi}[g_{i,u}(\theta)\ln g_{i,u}(\theta) - g_{i,u}(\theta)+1]d\theta. \quad (3)$$

All three entropies are quantified relative to completely disordered ideal gases of the same density, so that a negative value of entropy indicates local structural order.

To investigate the correlations between structural entropies and local dynamics, we measure particle dynamics using the local Debye-Waller factor $\sigma^2 = \langle[r_i(t)-\bar{r}_i]^2\rangle$ over a preselected time window τ. Here, $r_i(t)$ is the position of particle i at time t, $\bar{r}_i$ is the average position of particle, $\langle.\rangle$ denotes the time average [55,56]. The time window τ is selected to be the α-relaxation time of the system, when the highest correlations between structural entropies and dynamics are observed [47]. To ensure that entropies obtained from samples of different packing fractions are statistically comparable, the number of frames used calculating the distribution functions are fixed to be 36, the number of frames for τ_α in the most dilute sample. For samples of higher packing fractions, 36 equally spaced images are extracted from a video segment. A total of 150 segments are used for each packing fraction. For low packing fractions ($\phi < 0.77$), the segments are nonoverlapping; while for high packing fractions ($\phi \geq 0.77$), the segments are allowed to overlap [47].

Figure 2(a) plots a snapshot of the spatial distribution of σ^2 at $\phi = 0.83$. The particles are colored according to their percentile in σ^2, with warmer colors corresponding to particles with faster dynamics. For comparison, the spatial distributions of the structural entropies are shown in Figs. 2(b)–2(d). Both S_a and S_o exhibit clear spatial correlations to particle dynamics, with fast regions overlapping with regions with high structural entropy, or less local order. The correlation between S_2 and local dynamics, on the other hand, is considerably less obvious.

We quantify the correlations between local structural orders and dynamics by calculating the rank correlation

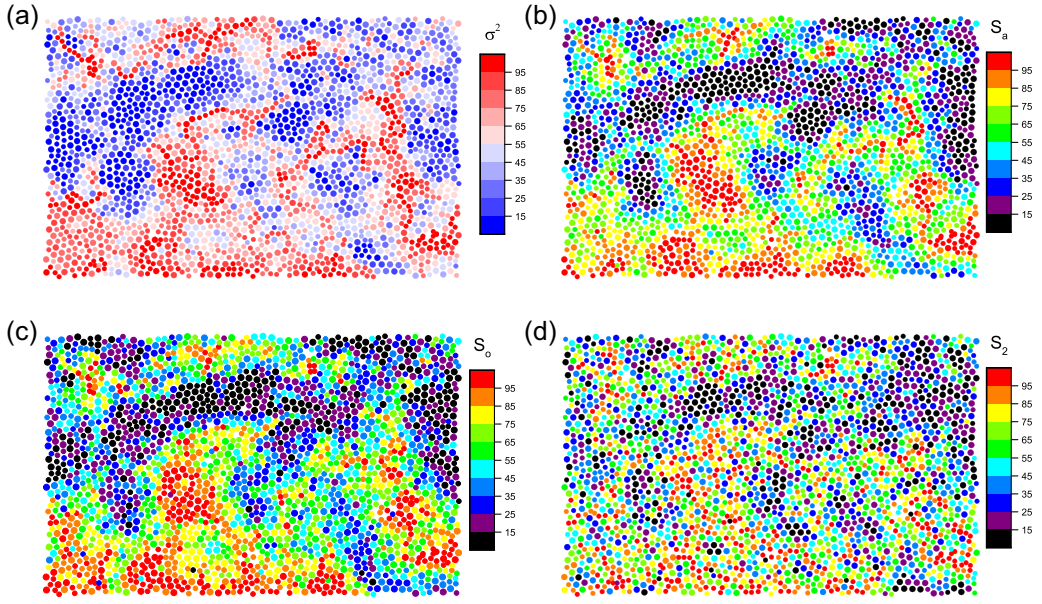

FIG. 2. Spatial distributions of dynamics and structural entropies. (a) Spatial distribution of σ^2 at $\phi = 0.83$. (b)–(d) Spatial distributions of $S_{a,i}$, $S_{o,i}$, and $S_{2,i}$, respectively. The particles are color-coded according to their percentile in the corresponding distributions.

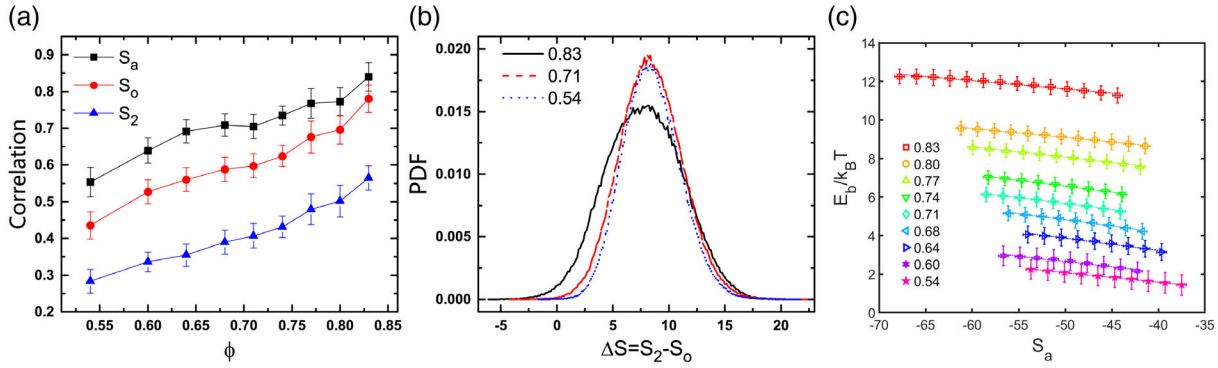

FIG. 3. Structural entropies and local dynamics. (a) Rank correlation coefficients between structural entropies and σ^2. (b) Distributions of the differences between S_2 and S_o for three different packing fractions. (c) Estimated activation energy barrier E_b as a function of S_a for large particles in different packing fractions; the dashed lines are linear fits to the experimental data.

coefficient [35] between structural entropies and σ^2. The experimental data are divided into separate segments of τ duration. For each segment, σ^2 and structural entropies are evaluated for each particle, and a rank correlation coefficients is calculated. The correlation coefficients from each segment are then averaged over all the segments. The total number of bins of the distributions used to calculate the structural entropies is fixed to be 600, so that the structural entropies and the corresponding correlations coefficients can be compared quantitatively [47]. Figure 3(a) plots the Spearman's rank correlation coefficients between local dynamics and S_a, S_2, and S_o, respectively, for the range of packing fractions across the glass transition. The error bars are the standard deviations of the correlation coefficients from different segments at a certain packing fraction. Of the three local structural order parameters, S_a shows the highest correlation to local dynamics, and S_2 the lowest, while the orientational entropy S_o falls in between. And for all three structural entropies, the average correlation to local dynamics increases with the packing fraction. At the highest packing fraction, $\sigma^2 - S_{a,i}$, correlation reaches a value greater than 0.8. Even at the lowest packing fraction of 0.55, where the particles are diffusing freely, $\sigma^2 - S_{a,i}$ still maintains a correlation coefficient of 0.55, greater than the highest correlation between σ^2 and S_2 at $\phi = 0.83$. Similarly high correlations between dynamics and orientational entropies have also been observed in simulations of 2D and 3D disordered packings, where orientational entropies S_a and S_o consistently outperform the direct two-body entropy S_2 [47].

The correlation coefficients between the structural entropies and local dynamics indicate the amount of information contained in the structural order parameters that is relevant to dynamics. Among the three structural parameters considered, S_a contains the most complete information on local structures, and naturally exhibits the highest correlation to dynamics at all packing fractions. The orientational entropy S_o and two-body entropy S_2 both miss about "half" of the structural information by averaging out the radial or angular component of the local distribution function. Naively, one might expect them to have similar decreases of correlations to dynamics compared to S_a. However, as shown in Fig. 3(a), the orientational entropy S_o consistently outperforms S_2 in correlating to local dynamics by more than 47.6%. This observation suggests that the structural orders in liquids or glasses consist mainly of orientational order, and local structures are more ordered orientationally than radially. Figure 3(b) plots the distribution of the difference between S_2 and S_o for different packing fractions. The S_2 values are systematically higher than S_o, indicating that local particles are indeed more uniformly distributed (thus less ordered) radially than orientationally. In addition, S_a and S_o also outperform a number of popular metrics applicable to experiments in correlating to local dynamics [47].

In the supercooled liquids, the activated local dynamics depends on the effective temperature T_{eff} that is inversely proportional to the packing fraction, and the local energy barrier E_b. The positive correlations between structural entropies and local dynamics suggest that more ordered structures correspond to slower dynamics, therefore higher activation barriers. According to Arrhenius-Kramers equation [57,58], local diffusion coefficients are directly related to the activation energy barrier by $(D_0/D) = \frac{4}{3}(2\pi k_B T/\sqrt{U_0''|U_b''|}\lambda^2)\exp(E_b/k_B T)$, where D_0 is the free diffusion coefficient, λ is the lattice constant, $U_0'' \equiv [d^2U(x)/dx^2]|_{x=x_0}$ and $U_b'' \equiv [d^2U(x)/dx^2]|_{x=x_b}$ are the second derivatives of dynamic free energy $U(x)$ [47]. In our experiments, the local diffusion coefficients D of a particle is estimated by σ_i^2/τ_α and λ is replaced by the mean separation of particles. Thus the local activation barrier can be obtained using $(E_b/k_B T) = \ln[\frac{3}{4}(\sqrt{U_0''|U_b''|}\lambda^2/2\pi k_B T)\times (D_0/D)]$. Figure 3(c) plots the energy barriers as a function of local structural entropies. The activation barrier decreases linearly with the structural entropy and the relative energy barrier between two distinct local structural entropies is almost independent of packing fractions [47].

In the experiments, the measured σ^2 consists of activated fluctuations and thermal noises independent of local barriers. At low packing fractions (high T_{eff}), the energy barriers are small compare to T_{eff}, and structure-dynamics correlation is degraded by the significant random noises. At higher packing fractions (low T_{eff}), the thermal noise is reduced, and local dynamics are largely determined by local structural orders, which results in higher $\sigma^2 - S$ correlations.

In summary, our current work quantifies structural orders in supercooled liquids and glasses using local distribution functions that include complete or partial structural information. Based on the general principle that structural orders are a reflection of spatial inhomogeneity of particle distributions, this method overcomes the lack of characteristic structural features in glassy materials, which has long frustrated the search for amorphous orders. The high correlations between the structural entropies and local dynamics shows that these structural parameters are indeed proper measures of order in local structures that can be quantitatively associated to the activation barriers in glasses. In particular, we show that orientational order is the main component of amorphous orders in both liquids and glasses when long-range structural correlation is absent. Structural entropies employed in the current work are an intuitive and simple way to identify orders in glass materials. Other constructions may also efficiently capture the spatial inhomogeneities in disordered packings, which should be the topic of future studies.

We thank Xiaoguang Ma and Hanbo Yang for the help in data analysis. We acknowledge the support from National Natural Science Foundation of China (Grants No. 12174434, No. 11874395). This work was also supported by the Strategic Priority Research Program of Chinese Academy of Sciences (Grant No. XDB33000000).

*These authors contributed equally to this work.
†Corresponding author: kechen@iphy.ac.cn

[1] A. van Blaaderen and P. Wiltzius, Science **270**, 1177 (1995).
[2] A. Cavagna, Phys. Rep. **476**, 51 (2009).
[3] N. Lačević, F. W. Starr, T. Schrøder, and S. C. Glotzer, J. Chem. Phys. **119**, 7372 (2003).
[4] Z. Zhang, P. J. Yunker, P. Habdas, and A. G. Yodh, Phys. Rev. Lett. **107**, 208303 (2011).
[5] A. S. Keys, A. R. Abate, S. C. Glotzer, and D. J. Durian, Nat. Phys. **3**, 260 (2007).
[6] O. Dauchot, G. Marty, and G. Biroli, Phys. Rev. Lett. **95**, 265701 (2005).
[7] W. Kob, C. Donati, S. J. Plimpton, P. H. Poole, and S. C. Glotzer, Phys. Rev. Lett. **79**, 2827 (1997).
[8] W. K. Kegel and A. van Blaaderen, Science **287**, 290 (2000).
[9] E. R. Weeks, J. C. Crocker, A. C. Levitt, A. Schofield, and D. A. Weitz, Science **287**, 627 (2000).
[10] L. Berthier, G. Biroli, J. P. Bouchaud, L. Cipelletti, D. E. Masri, D. L'Hote, F. Ladieu, and M. Pierno, Science **310**, 1797 (2005).
[11] L. Berthier, G. Biroli, J.-P. Bouchaud, L. Cipelletti, and W. van Saarloos, *Dynamical Heterogeneities in Glasses, Colloids, and Granular Media* (Oxford University Press, Oxford, 2011), Vol. 150.
[12] L. Berthier and G. Biroli, Rev. Mod. Phys. **83**, 587 (2011).
[13] M. D. Ediger, Annu. Rev. Phys. Chem. **51**, 99 (2000).
[14] A. Hirata, P. Guan, T. Fujita, Y. Hirotsu, A. Inoue, A. R. Yavari, T. Sakurai, and M. Chen, Nat. Mater. **10**, 28 (2011).
[15] Y. Yang, J. Zhou, F. Zhu, Y. Yuan, D. J. Chang, D. S. Kim, M. Pham, A. Rana, X. Tian, Y. Yao *et al.*, Nature (London) **592**, 60 (2021).
[16] C. P. Royall and S. R. Williams, Phys. Rep. **560**, 1 (2015).
[17] H. Tanaka, T. Kawasaki, H. Shintani, and K. Watanabe, Nat. Mater. **9**, 324 (2010).
[18] H. Sheng, W. Luo, F. Alamgir, J. Bai, and E. Ma, Nature (London) **439**, 419 (2006).
[19] K. F. Kelton, G. W. Lee, A. K. Gangopadhyay, R. W. Hyers, T. J. Rathz, J. R. Rogers, M. B. Robinson, and D. S. Robinson, Phys. Rev. Lett. **90**, 195504 (2003).
[20] Y. Hu, F. Li, M. Li, H. Bai, and W. Wang, Nat. Commun. **6**, 8310 (2015).
[21] R. Milkus and A. Zaccone, Phys. Rev. B **93**, 094204 (2016).
[22] G. Biroli, J.-P. Bouchaud, A. Cavagna, T. S. Grigera, and P. Verrocchio, Nat. Phys. **4**, 771 (2008).
[23] K. Hima Nagamanasa, S. Gokhale, A. Sood, and R. Ganapathy, Nat. Phys. **11**, 403 (2015).
[24] B. Zhang and X. Cheng, Phys. Rev. Lett. **116**, 098302 (2016).
[25] G. M. Hocky, T. E. Markland, and D. R. Reichman, Phys. Rev. Lett. **108**, 225506 (2012).
[26] J. Russo and H. Tanaka, Proc. Natl. Acad. Sci. U.S.A. **112**, 6920 (2015).
[27] E. D. Cubuk, S. S. Schoenholz, E. Kaxiras, and A. J. Liu, J. Phys. Chem. B **120**, 6139 (2016).
[28] E. D. Cubuk, S. S. Schoenholz, J. M. Rieser, B. D. Malone, J. Rottler, D. J. Durian, E. Kaxiras, and A. J. Liu, Phys. Rev. Lett. **114**, 108001 (2015).
[29] S. S. Schoenholz, E. D. Cubuk, D. M. Sussman, E. Kaxiras, and A. J. Liu, Nat. Phys. **12**, 469 (2016).
[30] E. D. Cubuk, R. Ivancic, S. S. Schoenholz, D. Strickland, A. Basu, Z. Davidson, J. Fontaine, J. L. Hor, Y.-R. Huang, Y. Jiang *et al.*, Science **358**, 1033 (2017).
[31] X. Ma, Z. S. Davidson, T. Still, R. J. S. Ivancic, S. S. Schoenholz, A. J. Liu, and A. G. Yodh, Phys. Rev. Lett. **122**, 028001 (2019).
[32] X. Yang, R. Liu, M. Yang, W.-H. Wang, and K. Chen, Phys. Rev. Lett. **116**, 238003 (2016).
[33] T. Kawasaki, T. Araki, and H. Tanaka, Phys. Rev. Lett. **99**, 215701 (2007).
[34] Z. Zheng, R. Ni, F. Wang, M. Dijkstra, Y. Wang, and Y. Han, Nat. Commun. **5**, 3829 (2014).
[35] H. Tong and H. Tanaka, Phys. Rev. X **8**, 011041 (2018).
[36] H. Tong and H. Tanaka, Phys. Rev. Lett. **124**, 225501 (2020).
[37] H. Tong and H. Tanaka, Nat. Commun. **10**, 5596 (2019).

[38] H. Tanaka, Eur. Phys. J. E **35**, 113 (2012).
[39] P. M. Chaikin, T. C. Lubensky, and T. A. Witten, *Principles of Condensed Matter Physics* (Cambridge University Press, Cambridge, England, 1995), Vol. 10.
[40] P. J. Yunker, K. Chen, M. D. Gratale, M. A. Lohr, T. Still, and A. Yodh, Rep. Prog. Phys. **77**, 056601 (2014).
[41] K. Chen, W. G. Ellenbroek, Z. Zhang, D. T. N. Chen, P. J. Yunker, S. Henkes, C. Brito, O. Dauchot, W. Van Saarloos, A. J. Liu *et al.*, Phys. Rev. Lett. **105**, 025501 (2010).
[42] K. Chen, M. L. Manning, P. J. Yunker, W. G. Ellenbroek, Z. Zhang, A. J. Liu, and A. G. Yodh, Phys. Rev. Lett. **107**, 108301 (2011).
[43] B. Bernu, Y. Hiwatari, and J. Hansen, J. Phys. C **18**, L371 (1985).
[44] R. Kurita and E. R. Weeks, Phys. Rev. E **82**, 041402 (2010).
[45] T. Hamanaka and A. Onuki, Phys. Rev. E **74**, 011506 (2006).
[46] J. C. Crocker and D. G. Grier, J. Colloid Interface Sci. **179**, 298 (1996).
[47] See Supplemental Material at http://link.aps.org/supplemental/10.1103/PhysRevLett.131.128201 for additional experimental and calculation details, which includes Refs. [48–53].
[48] S. Plimpton, J. Comput. Phys. **117**, 1 (1995).
[49] D. Richard, M. Ozawa, S. Patinet, E. Stanifer, B. Shang, S. Ridout, B. Xu, G. Zhang, P. Morse, J.-L. Barrat *et al.*, Phys. Rev. Mater. **4**, 113609 (2020).
[50] J. M. Rieser, C. P. Goodrich, A. J. Liu, and D. J. Durian, Phys. Rev. Lett. **116**, 088001 (2016).
[51] C.-C. Chang and C.-J. Lin, ACM Trans. Intell. Syst. Technol. **2**, 1 (2011).
[52] A. Ghosh, V. K. Chikkadi, P. Schall, J. Kurchan, and D. Bonn, Phys. Rev. Lett. **104**, 248305 (2010).
[53] M. D. Gratale, P. J. Yunker, K. Chen, T. Still, K. B. Aptowicz, and A. G. Yodh, Phys. Rev. E **87**, 052301 (2013).
[54] D. C. Wallace, J. Chem. Phys. **87**, 2282 (1987).
[55] A. Widmer-Cooper and P. Harrowell, Phys. Rev. Lett. **96**, 185701 (2006).
[56] H. Tong and N. Xu, Phys. Rev. E **90**, 010401(R) (2014).
[57] X.-g. Ma, P.-Y. Lai, and P. Tong, Soft Matter **9**, 8826 (2013).
[58] X.-g. Ma, P.-Y. Lai, B. J. Ackerson, and P. Tong, Soft Matter **11**, 1182 (2015).